Optical excitation of zigzag carbon nanotubes with photons guided in nanofibers

S. Broadfoot,[1] U. Dorner,[2,1] and D. Jaksch[1,2]

[1]*Clarendon Laboratory, University of Oxford, Parks Road, Oxford OX1 3PU, United Kingdom*
[2]*Centre for Quantum Technologies, National University of Singapore, 117543, Singapore*

We consider the excitation of electrons in semiconducting carbon nanotubes by photons from the evanescent field created by a subwavelength-diameter optical fiber. The strongly changing evanescent field of such nanofibers requires dropping the dipole approximation. We show that this leads to novel effects, especially a high dependence of the photon absorption on the relative orientation and geometry of the nanotube-nanofiber setup in the optical and near-infrared domain. In particular, we calculate photon absorption probabilities for a straight nanotube and nanofiber depending on their relative angle. Nanotubes orthogonal to the fiber are found to perform much better than parallel nanotubes when they are short. As the nanotube gets longer the absorption of parallel nanotubes is found to exceed the orthogonal nanotubes and approach 100% for extremely long nanotubes. In addition, we show that if the nanotube is wrapped around the fiber in an appropriate way the absorption is enhanced. We find that optical and near-infrared photons could be converted to excitations with efficiencies that may exceed 90%. This may provide opportunities for future photodetectors and we discuss possible setups.

I. INTRODUCTION

The unique physical properties of carbon nanotubes and the flexibility they provide in selecting their characteristics offers great potential for nanotechnology.[1–3] Carbon nanotubes can be either semiconducting or metallic, depending on their diameter and helical configuration. They typically have nanometer-sized diameters and a length of a few microns, although centimeter long nanotubes have been produced recently.[4] This makes them ideal 1D systems that possess a ballistic conducting channel,[5] no backward scattering, and energy levels that can be adjusted with external fields.[6–8] Superconductivity has also been observed in multiwalled carbon nanotubes and single carbon nanotubes have exhibited a superconducting proximity effect.[9–12] Their applications range from extremely strong fibers and organic electronics[13] to electrochemical sensors[14,15] and photon detectors.[16]

Carbon nanotubes are a form of carbon formed by rolling up a sheet of graphene into a cylindrical tube. An illustration of this is given in Fig. 1. Here we focus on the optical properties of carbon nanotubes. For a straight nanotube, inside a weak uniform classical plane wave field, these properties have been extensively studied.[17–27] Their quasi-one-dimensionality means that their density of states exhibits Van Hove singularities and these contribute to strong optical absorption peaks. However, these results apply the dipole approximation, where it is assumed that the field does not vary along the nanotube's length. We extend this treatment by allowing for the spatial dependence of the field. This situation is particularly relevant when the electrons are delocalized in a tightly confined field, such that the field varies greatly over a few hundred nanometers. The degree to which the electrons are delocalized is a topic of ongoing research and various studies have been done on the coherence length in nanotubes. Their results range from 10 nm to several microns suggesting that the spatial field dependence is certainly important for confined fields and may also be relevant for plane waves.[28–32] The systems we are primarily interested in are subwavelength-diameter optical fibers coupled to carbon nanotubes. The electrical field of a

nanofiber is tightly confined and primarily exists outside of the fiber, in a large evanescent field.[33] Due to the presence of a strong field in a relativity small volume, these nanofibers are ideal candidates to achieve a high optical absorption in atomic systems. For example, their interaction with atom arrays has been studied.[34–36] However, in contrast to such atom-fiber systems, the dipole approximation cannot be applied in the case of nanotubes since the optical field typically changes rapidly along a nanotube's length. In this paper we calculate the (internal) quantum efficiency, i.e., the probability that a nanotube, placed inside the evanescent field of a nanofiber, absorbs a photon. Calculations for the external quantum efficiency, i.e., the efficiency for detecting the excitation with the photocurrent, are beyond the scope of this paper. However, it should be noted that important effects that could aid in this procedure, such as the avalanche effect, have been observed in carbon nanotubes.[37] We focus specifically on the example of zigzag nanotubes (see Fig. 1) because they can be direct semiconductors. However, our results are still representative of other semiconducting nanotube types such as chiral nanotubes. We find that the absorption is extremely dependent on the nanotube's orientation. These results are highly relevant for the interface between any future nanoscale photonics and carbon nanotubes. If the absorption process is coherent the system may also be suitable as a quantum memory, which maps a photonic quantum state onto a coherent excitation of the nanotube.

We will be using the band-to-band tight-binding transition model for the carbon nanotube. This has proven itself to be very effective in determining the basic optical properties of nanotubes but does not include effects due to excitons[38] and electron-electron interactions.[39] Such effects give measurable corrections and there have been a few studies considering the exciton absorption strength.[17,23,40,41] Nevertheless, the band-to-band model is suitable to determine the main contributions to optical absorption.

This paper is organized as follows. We begin by giving an overview of nanotube properties and the calculation of their band structure in Sec. II. Based on this we then evaluate the
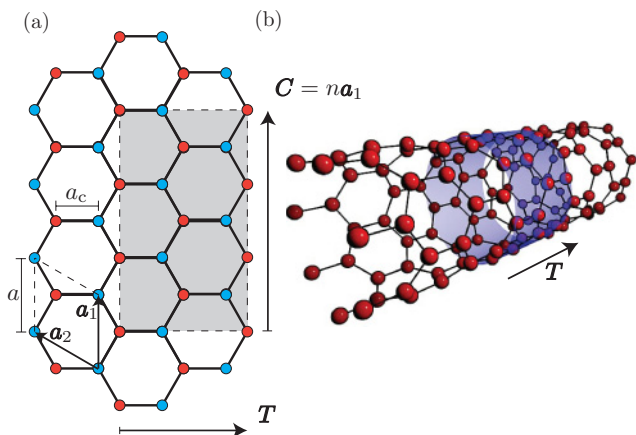
FIG. 1. (Color online) (a) Graphene lattice with the unit cells vectors labeled $\mathbf{a}_1$ and $\mathbf{a}_2$. These vectors have the length a. Here the atoms in the A sublattice are red (dark gray) and the B sublattice is cyan (light gray). a_c is the distance between neighboring atoms. The unwrapped unit cell for a zigzag (3,0) nanotube is shown shaded and the **C** vector defines the nanotube's circumference. (b) A section from a zigzag (7,0) nanotube is shown with its unit cell shaded. **T** is the tangential unit vector of the nanotube's unit cell.

photon absorption by zigzag carbon nanotubes in Sec. III. In the setups considered in this paper the nanotubes experience fields that change strongly along their length; i.e., to calculate photon absorption we cannot rely on the dipole approximation. We obtain general expressions for the absorption probability which are then applied to cylindrical vacuum-clad silica nanofibers in Sec. IV, and discuss different geometrical setups of nanofibers and nanotubes. Possible photodetectors that use these setups are then presented in Sec. V. Finally, in Sec. VI, we summarize our results.

II. THE TIGHT-BINDING MODEL FOR THE CARBON NANOTUBE

Here we will review the basic properties of carbon nanotubes for completeness and layout the notation that we use in later sections. A single-walled carbon nanotube (SWCNT) can be thought of as a sheet of graphene wrapped into a tube, so we will start by describing the tight-binding model of graphene.[42] Graphene is a regular 2D hexagonal Bravais lattice of carbon atoms and its structure is shown in Fig. 1. We label the unit vectors of the graphene lattice $\mathbf{a}_1$ and $\mathbf{a}_2$. The length of these vectors is the lattice constant a which is related to the distance between neighboring carbon atoms, a_c, by $a = \sqrt{3}a_c \simeq 0.246$ nm. Within each unit cell there are two carbon atoms, which we label to form the A and B sublattices. We can then define the unit vectors of the reciprocal lattice as $\mathbf{b}_1$ and $\mathbf{b}_2$, with $\mathbf{a}_i \cdot \mathbf{b}_j = 2\pi\delta_{ij}$. The first Brillouin zone given by these is also hexagonal. It has a selection of points with high symmetry: one at the center, the midpoints of the hexagonal edges, and two inequivalent types of corners.

The well-established tight-binding model assumes that the electrons are tightly bound to the individual carbon atoms and the localized atomic orbitals are used as a basis for expanding the wave function. We consider orbitals that contribute to states

that lie within an optical range of energies around the Fermi level. These are the states that give the main contributions to the optical properties of the nanotube. Every carbon atom has four valence orbitals ($2s$, $2p_x$, $2p_y$, and $2p_z$) that could lie in this energy range. For 2D graphene the (s, p_x, p_y) orbitals combine to form hybridized sp^2 orbitals. These give the strong covalent bonds, primarily responsible for the binding energy and elastic properties of the nanotubes. In the tight-binding model they result in σ and σ^* bands. However, their energy levels are far away from the Fermi level and hence they do not play a key role in the optical properties that we are interested in. That role is played by delocalized π and π^* bands that are formed from the p_z orbitals.[1] Hence, we can ignore the σ electrons and restrict the tight-binding model to the π electrons. The Hamiltonian for this system is

$$\hat{H}_0 = -\gamma_0 \sum_{ij}(\hat{\alpha}_i^\dagger \hat{\beta}_j + \text{H.c.}), \qquad (1)$$

where $-\gamma_0$ is the hopping amplitude and ij refers to nearest neighbors. Here, $\hat{\alpha}_i^\dagger$ and $\hat{\beta}_j^\dagger$ are the creation operators for electrons in sublattice A and B, respectively. In this Hamiltonian we have removed the constant energy contribution that corresponds to the Fermi level. We expand the wave function in terms of p_z orbitals at every atom site and split this expression into two parts, one for each sublattice. The wave function for each state is then

$$\Psi(\mathbf{k},\mathbf{r}) = \sum_{\mathbf{r}_A} C_A(\mathbf{r}_A,\mathbf{k})p_z(\mathbf{r}-\mathbf{r}_A) \qquad (2)$$

$$+ \sum_{\mathbf{r}_B} C_B(\mathbf{r}_B,\mathbf{k})p_z(\mathbf{r}-\mathbf{r}_B) \qquad (3)$$

with $\mathbf{r}_A, \mathbf{r}_B$ labeling the atom locations in sublattice A and B, respectively. The individual p_z orbitals are given by the normalized wave functions $p_z(\mathbf{r})$ and each one has a coefficient, represented with C_A and C_B. By using translational symmetry we can represent this as

$$\Psi(\mathbf{k},\mathbf{r}) = c_A(\mathbf{k})\tilde{p}_z^A(\mathbf{k},\mathbf{r}) + c_B(\mathbf{k})\tilde{p}_z^B(\mathbf{k},\mathbf{r}), \qquad (4)$$

where the Bloch functions, $\tilde{p}_z^A$ and $\tilde{p}_z^B$, are

$$\tilde{p}_z^A(\mathbf{k},\mathbf{r}) = \frac{1}{\sqrt{N_{\text{cells}}}} \sum_{\mathbf{r}_A} e^{i\mathbf{k}\cdot\mathbf{r}_A} p_z(\mathbf{r}-\mathbf{r}_A), \qquad (5)$$

$$\tilde{p}_z^B(\mathbf{k},\mathbf{r}) = \frac{1}{\sqrt{N_{\text{cells}}}} \sum_{\mathbf{r}_B} e^{i\mathbf{k}\cdot\mathbf{r}_B} p_z(\mathbf{r}-\mathbf{r}_B). \qquad (6)$$

Here N_{cells} is the number of unit cells in the graphene sheet. These Bloch functions have the coefficients c_A and c_B. The states are labeled by their crystal momentum vector $\mathbf{k}$. We now solve the time-independent single-particle Schrödinger equation

$$\hat{H}_0\Psi(\mathbf{k},\mathbf{r}) = E(\mathbf{k})\Psi(\mathbf{k},\mathbf{r}). \qquad (7)$$

We define the quantity

$$\phi_{\mathbf{k}} = \sum_{\mathbf{q}} e^{i\mathbf{k}\cdot\mathbf{q}}, \qquad (8)$$

where $\mathbf{q}$ are vectors from an atom in the A sublattice to its neighboring atoms in the B lattice. This gives us the following
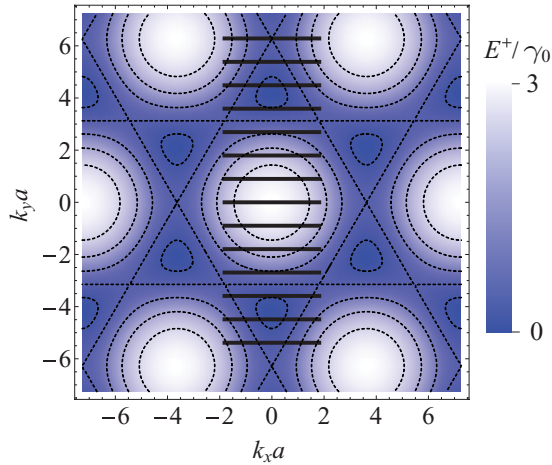
FIG. 2. (Color online) Graphene band structure and the locations of subbands for a (7,0) nanotube (black solid lines). The transitions between bands allowed with the electric field perpendicular to the nanotube can occur between neighboring subbands. The dashed lines are contours for E^+/γ_0 equal to 0.5, 1, 1.5, 2, and 2.5.

quantities:

$$
\begin{aligned}
H_{AA} = H_{BB} &= \langle \tilde{p}_z^A | \hat{H}_0 | \tilde{p}_z^A \rangle = \langle \tilde{p}_z^B | \hat{H}_0 | \tilde{p}_z^B \rangle = 0, \\
H_{AB} = H_{BA}^* &= \langle \tilde{p}_z^A | \hat{H}_0 | \tilde{p}_z^B \rangle = -\gamma_0 \phi_{\mathbf{k}}, \\
S_{AB} = S_{BA}^* &= \langle \tilde{p}_z^A | \tilde{p}_z^B \rangle = u \phi_{\mathbf{k}}.
\end{aligned}
\tag{9}
$$

Now the variational Schrödinger equation in matrix form is

$$
\begin{pmatrix} H_{AA} & H_{AB} \\ H_{BA} & H_{BB} \end{pmatrix} \begin{pmatrix} c_A \\ c_B \end{pmatrix} = E(\mathbf{k}) \begin{pmatrix} 1 & S_{AB} \\ S_{BA} & 1 \end{pmatrix} \begin{pmatrix} c_A \\ c_B \end{pmatrix}. \tag{10}
$$

The above matrix equation can be solved to give the energy of each state as

$$
E^\pm(\mathbf{k}) = \frac{\pm \gamma_0 |\phi_{\mathbf{k}}|}{1 \mp u |\phi_{\mathbf{k}}|}, \tag{11}
$$

where

$$
\begin{aligned}
|\phi_{\mathbf{k}}| &= \left[1 + 4 \cos\left(\frac{k_x a \sqrt{3}}{2} \right) \cos\left(\frac{k_y a}{2} \right) + 4 \cos^2\left(\frac{k_y a}{2} \right) \right]^{1/2}.
\end{aligned}
\tag{12}
$$

A typical value for γ_0 is 2.89 eV such that the tight-binding model corresponds with experiments.[3,43,44] We will keep u in the equations but for all plots and numerical calculations we assume that $u = 0$; i.e., there is no orbital overlap. In Fig. 2 this 2D dispersion relation is plotted as a contour. In Eq. (11) the signs refer to the two relevant bands, the conduction band and the valence band. The coefficients are found to be

$$
c_A^v(\mathbf{k}) = \sqrt{\frac{\phi_{\mathbf{k}}}{2|\phi_{\mathbf{k}}|(1 + u|\phi_{\mathbf{k}}|)}}, \tag{13}
$$

$$
c_B^v(\mathbf{k}) = \sqrt{\frac{\phi_{\mathbf{k}}^*}{2|\phi_{\mathbf{k}}|(1 + u|\phi_{\mathbf{k}}|)}}, \tag{14}
$$

$$
c_A^c(\mathbf{k}) = -\sqrt{\frac{\phi_{\mathbf{k}}}{2|\phi_{\mathbf{k}}|(1 - u|\phi_{\mathbf{k}}|)}}, \tag{15}
$$

$$
c_B^c(\mathbf{k}) = \sqrt{\frac{\phi_{\mathbf{k}}^*}{2|\phi_{\mathbf{k}}|(1 - u|\phi_{\mathbf{k}}|)}}. \tag{16}
$$

Now we know the relevant band structure of graphene and its wave functions; we need to obtain the energy states of the nanotubes. To do this we use the zone-folding approximation. This assumes the nanotube bands are the same as graphene but with limited $\mathbf{k}$, due to the 1D nature of a carbon nanotube. There are a variety of ways available to wrap the sheet up into a nanotube, each of which results in very different properties. The nanotubes are characterized by a vector in the graphene plane that corresponds to the circumference of the nanotube and is called the chiral vector $\mathbf{C} = n_1 \mathbf{a}_1 + n_2 \mathbf{a}_2$ ($0 \leqslant |n_2| \leqslant n_1$) (see Fig. 1). It gives the relative position of two graphene atoms that become "identical" when the graphene is rolled into a nanotube. We will use these parameters in the standard form (n_1, n_2) to label each type of nanotube. This immediately defines some basic geometric properties such as the tube's circumference and radius $R_t = a\sqrt{n_1^2 + n_1 n_2 + n_2^2}/2\pi$. We also define the translational vector, perpendicular to $\mathbf{C}$, that corresponds to the direction along the tube, $\mathbf{T} = t_1 \mathbf{a}_1 + t_2 \mathbf{a}_2$. Using the greatest common divisor (gcd), we define $t_1 = (2n_2 + n_1)/N_R$, $t_2 = -(2n_1 + n_2)/N_R$, and $N_R = \gcd(2n_1 + n_2, 2n_2 + n_1)$. The two vectors, $\mathbf{C}$ and $\mathbf{T}$, define the unit cell of the nanotube. Within each nanotube unit cell there are $N_G = 2(n_1^2 + n_1 n_2 + n_2^2)/N_R$ graphene unit cells and, hence, $N_C = 2N_G$ carbon atoms. In a nanotube of length L there are $N_L = L/|\mathbf{T}|$ nanotube unit cells. For the nanotube's reciprocal lattice we define $\mathbf{K}_1 = (t_1 \mathbf{b}_2 - t_2 \mathbf{b}_1)/N_G$ and $\mathbf{K}_2 = (n_2 \mathbf{b}_1 - n_1 \mathbf{b}_2)/N_G$ such that $\mathbf{K}_1 \cdot \mathbf{T} = \mathbf{K}_2 \cdot \mathbf{C} = 0$ and $\mathbf{K}_1 \cdot \mathbf{C} = \mathbf{K}_2 \cdot \mathbf{T} = 2\pi$. These give the allowed vectors in the SWCNT's Brillouin zone to be a set of N_G 1D "cutting lines" with values

$$
\mathbf{k} = \mu \mathbf{K}_1 + k_{||} \frac{\mathbf{K}_2}{|\mathbf{K}_2|}, \tag{17}
$$

with $\mu = -N_G/2 + 1, \dots, 0, \dots, N_G/2$ and $-\pi/|\mathbf{T}| \leqslant k_{||} < \pi/|\mathbf{T}|$. It is the periodic boundary condition along the circumferential direction of the tube that causes the wave vector to become quantized and each discrete cutting line is labeled by the azimuthal quantum number μ. For short nanotubes the wave vectors are also quantized along the nanotube's length causing discrete energy levels to be formed.[45] These discrete values have $k_{||} = 2\pi j/L - \pi/|\mathbf{T}|$, for an integer $j = 1, \dots, N_L$. Local effects also occur in short nanotubes, such as a sharp spike in the density of states (DOS), caused by defects at the caps. Such effects will be ignored here. Typically, the nanotube is assumed to be of infinite length, allowing continuous values of the wave vector along the nanotube axis. This causes possible wave vectors to lie in "subbands." The subbands can cut through the Fermi points of graphene causing the tube to become metallic. This can be shown to be the case for nanotubes of the type (n,m), where $n - m$ is a multiple of three. If this is not the case there is a nonzero band gap and the nanotube is semiconducting. Here we consider "zigzag" semiconducting nanotubes of the form $(n,0)$, with n not a multiple of three. The discrete wave vectors are then

$$
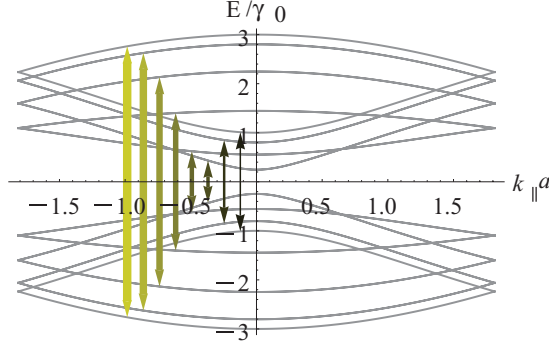|k_\perp| = \frac{2\pi \mu}{|\mathbf{C}|} \tag{18}
$$

FIG. 3. (Color online) The dispersion relation for a (7,0) nanotube. The possible transitions caused by light linearly polarized parallel to the nanotube are shown by arrows. These arrows only represent the transition between subbands and their horizontal positions have no meaning. Here the band gap is 1.43 eV, when γ_0 is taken as 2.89 eV.

with $\mu = -(n-1), \ldots, 0, 1, 2, \ldots, n$ and

$$|k_{||}| < \frac{\pi}{|\mathbf{T}|}. \tag{19}$$

The momentum vectors associated with these subbands are highlighted in Fig. 2 for a (7,0) nanotube. For zigzag nanotubes $k_\perp$ corresponds to k_y and $k_{||}$ corresponds to k_x. It should be noted that subbands μ and $-\mu$ both have the same energy and this degeneracy is referred to as the "valley" degeneracy. Combined with the two electron spins this gives a degeneracy of four for each energy value, except for $\mu = 0$ and $\mu = n$ that only have spin degeneracy. The energy of the subbands is

$$E_{NT}^\pm(k_{||}, \mu) = E^\pm\left(k_{||}\frac{\mathbf{K}_2}{|\mathbf{K}_2|} + \mu\mathbf{K}_1\right). \tag{20}$$

These are plotted for a (7,0) nanotube in Fig. 3, which has a band gap of 1.43 eV.

III. THE OPTICAL ABSORPTION OF CARBON NANOTUBES

The Hamiltonian of a nanotube interacting with an electromagnetic field is $\hat{H} = \hat{H}_0 + \hat{H}_F + \hat{H}_I$, with

$$\hat{H}_I = \frac{e}{m_e}\hat{\mathbf{A}} \cdot \hat{\mathbf{p}} \tag{21}$$

being the interaction term and $\hat{H}_F$ representing the field Hamiltonian. Here, we define e as the magnitude of the electron charge and are using SI units. Each field mode is characterized by its angular frequency ω and further parameters, which define the mode's polarization and propagation direction. The field vector potential operator is

$$\hat{\mathbf{A}} = \int_0^\infty d\omega(\hat{\mathbf{A}}_\omega^+ e^{-i\omega t} + \hat{\mathbf{A}}_\omega^- e^{i\omega t}). \tag{22}$$

We will consider the initial and final state of field to be a coherent monochromatic state $|\alpha_{\omega_0}\rangle$, with an angular frequency of ω_0 and a mean photon flux of F photons per unit time. This state satisfies the equation $\hat{a}_\omega|\alpha_{\omega_0}\rangle = \alpha|\alpha_{\omega_0}\rangle$, with $\alpha = \sqrt{2\pi F}\delta(\omega - \omega_0)$ and $\hat{a}_\omega$ being the field mode's destruction

operator.[46] This allows us to give

$$\mathbf{A} = \langle\alpha_{\omega_0}|\hat{\mathbf{A}}|\alpha_{\omega_0}\rangle \tag{23}$$

$$= \mathbf{A}^+ e^{-i\omega_0 t} + \mathbf{A}^- e^{i\omega_0 t}. \tag{24}$$

Using time-dependent perturbation theory we find that after time t, the initial state of the nanotube and field, $|\Psi^v\rangle|\alpha_{\omega_0}\rangle$, is in the state $|\Psi'^c\rangle|\alpha_{\omega_0}\rangle$ with probability

$$P = t\frac{2\pi}{\hbar}\left|\langle\Psi'^c|\left(\frac{e}{m_e}\mathbf{A}^+ \cdot \hat{\mathbf{p}}\right)|\Psi^v\rangle\right|^2 \delta(E' - E - \hbar\omega_0), \tag{25}$$

which is Fermi's golden rule. The transition rate for each electron in the state with energy E to each state with energy E' can be expressed as

$$w = \frac{2\pi}{\hbar}\left|\frac{e}{m_e}i\hbar G\right|^2 \delta(E' - E - \hbar\omega_0). \tag{26}$$

To calculate the optical absorption of a carbon nanotube of length L, the interaction term, $i\hbar G = i\hbar\langle\Psi'^c|\mathbf{A}^+ \cdot \nabla|\Psi^v\rangle$, needs to be found with spatially changing field. Here we are assuming that the state is coherent over the entire length of the nanotube. To calculate G we define

$$\mathbf{v}^A(\mathbf{k}) = \sum_{\mathbf{q}} e^{i\mathbf{k}\cdot\mathbf{q}}\mathbf{q}, \tag{27}$$

$$\mathbf{v}^B(\mathbf{k}) = -\sum_{\mathbf{q}} e^{-i\mathbf{k}\cdot\mathbf{q}}\mathbf{q}, \tag{28}$$

with $\mathbf{q}$ summing over the three vectors pointing from an atom in the A sublattice to its neighboring three B lattice atoms. We will furthermore use the matrix element, $M = \langle p_z(\mathbf{r})|\nabla_z|p_z(\mathbf{r} - \mathbf{q}_z)\rangle$, with $\mathbf{q}_z$ being the vector between two neighboring atoms such that the z axis is aligned along $\mathbf{q}_z$. The value we will later use for this is given by[25]

$$M = 2a\gamma_0 m_e/\hbar^2\sqrt{3}. \tag{29}$$

Each of the unit cells in the nanotube extends over a distance of $|\mathbf{T}| \approx 0.43$ nm along the nanotube and approximately a nanometer across. This is much smaller than the light's wavelength and spatial variations. Therefore, we can assume that the electromagnetic field is constant across each of the nanotube's unit cells. There are N_L of these unit cells along the nanotube's length and in each one, labeled by an integer l, the field is given by $\mathbf{A}_l^+ = \mathbf{A}^+(l|\mathbf{T}| - L/2)$.

An expression for G can then be calculated and simplified into the form (see Appendix A)

$$G = \frac{1}{N_L}\mathbf{D}(\mathbf{k}',\mathbf{k}) \cdot \left[\sum_{l=1}^{N_L} e^{i(al\sqrt{3} - L/2)(k_{||} - k'_{||})}\mathbf{A}_l^+\right] \tag{30}$$

$$\approx \frac{1}{L}\mathbf{D}(\mathbf{k}',\mathbf{k}) \cdot \left[\int_{l=-L/2}^{L/2} dl\, e^{il(k_{||} - k'_{||})}\mathbf{A}^+(l)\right], \tag{31}$$

where

$$\begin{aligned}
D_z = \frac{M\sqrt{3}}{2an}\sum_{j=1}^n \Big[&c_A^{c*}(\mathbf{k}')c_B^v(\mathbf{k})e^{-ija(k'_\perp - k_\perp)} \\
&\times (1 + e^{-ia(\mathbf{k}' - \mathbf{k})\cdot(\sqrt{3}/2, 1/2)})v_z^A(\mathbf{k}) \\
&- c_B^{c*}(\mathbf{k}')c_A^v(\mathbf{k})e^{-ija(k'_\perp - k_\perp)}e^{-ia(k'_{||} - k_{||})/\sqrt{3}} \\
&\times (1 + e^{-ia(\mathbf{k}' - \mathbf{k})\cdot(\sqrt{3}/2, 1/2)})v_z^A(\mathbf{k})^* \Big],
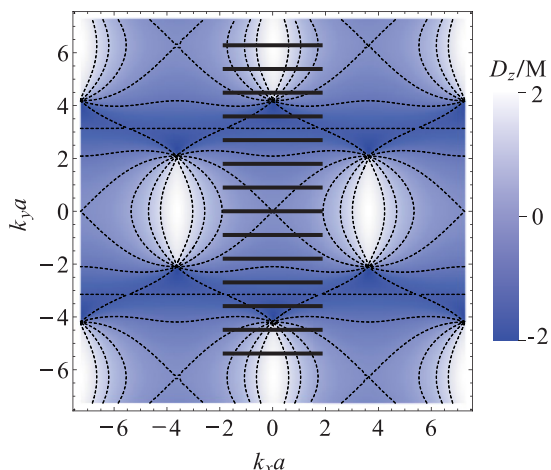\end{aligned} \tag{32}$$

and $D_{x,y}$ are given in Appendix A.

FIG. 4. (Color online) A density plot of $D_z(\mathbf{k},\mathbf{k})$ for graphene is shown together with the nanotube's subband lines (black solid lines) and contours (dashed lines) for values of D_z/M equal to -1, $-0.5, 0, 0.5, 1$, and 1.5. It is given in terms of the constant M from Eq. (29).

This result coincides with that of Ref. 18 when $\mathbf{A}_l^+$ is the same for all l. In Eq. (31) the $\mathbf{D}$ gives the selection rules for possible transitions between bands μ' and μ. In particular $D_z(\mathbf{k}',\mathbf{k})$ is negligible if $\mu' \neq \mu$ and for the other components of $\mathbf{D}(\mathbf{k}',\mathbf{k})$ to contribute we require $\mu' = \mu \pm 1$. For a uniform field across the nanotube these give the possible transitions for a field polarized parallel and perpendicular to the nanotube, respectively. In Fig. 4 we have plotted $D_z(\mathbf{k},\mathbf{k})$, and in Fig. 5 $D_{x,z}$ is plotted. These expressions correspond to direct transitions, i.e., with $k'_{||} = k_{||}$, which is an approximation of momentum conservation and will be discussed later in this section.

Although the values of D_x and D_y show a transition, the induced local field creates a depolarization effect[47–49] that reduces D_x and D_y to give a negligible contribution to the absorption. This allows us to focus on the D_z term and simplify G to

$$G \approx \frac{1}{L} D_z(\mathbf{k}',\mathbf{k}) \left[\oint \mathbf{A}^+ \cdot \mathbf{dr} e^{is(k_{||} - k'_{||})} \right], \quad (33)$$

with s denoting the length along the nanotube. This also restricts the transitions to those with $\mu' = \mu$.
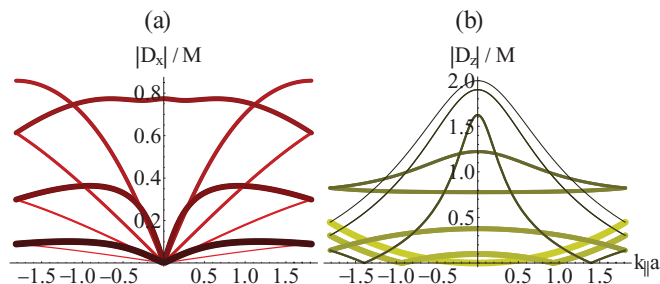

FIG. 5. (Color online) (a) D_x values for the different transitions that can occur when the electric field is perpendicular to the nanotube. M is given by Eq. (29). (b) D_z for transitions allowed with an electric field parallel to the nanotube. The thickness and color for each transition has been made to match the arrows used in Fig. 3.

It is the line integral in Eq. (33) that is responsible for momentum conservation in the system. The photon momentum is much smaller than the crystal momentum and typically only direct transitions are considered; i.e., $k'_{||} \approx k_{||}$. Here we will make this assumption; however, the change in momentum cannot be completely neglected since any change can make a major difference to the line integral in Eq. (33). This is especially true when the field oscillates along the nanotube. The energy of a direct transition is given by $E_g(\mathbf{k}) = E^+(\mathbf{k}) - E^-(\mathbf{k})$. Since $D_z(\mathbf{k}',\mathbf{k}) \approx D_z(\mathbf{k},\mathbf{k})$, when $k'_{||} \approx k_{||}$, we will make this substitution and further simplify $D_z(\mathbf{k},\mathbf{k}) = D_z(\mathbf{k})$ to give

$$D_z(\mathbf{k}) = \frac{-M\sqrt{3}}{a} \text{Re}\left(v_z^A(\mathbf{k}) \frac{\phi_{\mathbf{k}}^*}{|\phi_{\mathbf{k}}|\sqrt{1 - u^2 |\phi_{\mathbf{k}}|^2}} \right). \quad (34)$$

We define $A_{||}^+(s)ds = \mathbf{A}^+ \cdot \mathbf{dr}$ to be the field potential along the nanotube and use the discrete momentum values, $k_{||} = 2\pi j/L$ and $k'_{||} = 2\pi j'/L$, with integers j and j'. The line integral can then be expressed as

$$S(k_{||} - k'_{||}) = (1/L) \oint \mathbf{A}^+ \cdot \mathbf{dr} e^{is(k_{||} - k'_{||})} \quad (35)$$

$$= (1/L) \int_{-L/2}^{L/2} ds\, A_{||}^+(s) e^{is(k_{||} - k'_{||})} \quad (36)$$

$$= (1/L) \int_{-L/2}^{L/2} ds\, A_{||}^+(s) e^{i2\pi s(j - j')/L}. \quad (37)$$

This expression is simply the coefficient in the Fourier series for $A_{||}^+(s)$. Since the photon momentum is very small in comparison to the crystal momentum the only relevant coefficients will have very small values of $j' - j$ relative to N_L. Every electron transition in the nanotube then needs to be considered to calculate the overall absorption rate. This leads to a length dependence on the absorption. We initially consider discrete states and corresponding $k_{||}$ values. The transition rate given by Eq. (26) is summed over all possible initial and final states to give

$$w_L \approx \sum_{d_i} \sum_{\mu=-n+1}^{n} \sum_{k_{||}} \sum_{k'_{||}} \frac{2\pi\hbar e^2}{m_e^2} |D_z(\mathbf{k})|^2$$
$$\times |S(k_{||} - k'_{||})|^2 \delta(E_g(\mathbf{k}) - \hbar\omega_0). \quad (38)$$

In this equation d_i refer to the degeneracy of the initial state. For any value of $k_{||}$ the sum over $k'_{||}$ causes $k_{||} - k'_{||}$ to take all of the low values that are relevant. This sum is also independent of $k_{||}$ and allows us to define $S = \sum_j |S(2\pi j/L)|^2$, which can be rewritten using Parseval's theorem to be

$$S = (1/L) \int_{-L/2}^{L/2} ds\, |A_{||}^+(s)|^2. \quad (39)$$

The total absorption rate is then

$$w_L \approx \sum_{d_i} \sum_{\mu=-n+1}^{n} \sum_{k_{||}} \frac{2\pi\hbar e^2}{m_e^2} |D_z(\mathbf{k})|^2 S\delta(E_g(\mathbf{k}) - \hbar\omega_0) \quad (40)$$

$$\approx U(\omega_0) \int_{-L/2}^{L/2} ds\, |A_{||}^+(s)|^2, \quad (41)$$

where we define

$$U(\omega_0) = \sum_{d_i} \sum_{\mu=-n+1}^{n} \int dk_{||} \frac{\hbar e^2}{m_e^2} |D_z(\mathbf{k})|^2 \delta(E_g(\mathbf{k}) - \hbar\omega_0).$$

(42)

The field was defined to be a coherent state with a photon flux given by F photons per unit time. We divide the transition rate, given in Eq. (41), by this flux to obtain an estimate for the probability of one photon exciting a single electron. This expression gives a probability that increases linearly with nanotube length. This is certainly suitable up to the coherence length L_c, however not for long nanotubes. So far we have considered the length of the nanotube to be smaller than the coherence length. For long nanotubes we can consider the whole nanotube to be composed of coherent segments. This leads to an exponential increase in the absorption with the nanotube length. Here, to calculate this quantity we find the probability of not exciting any electrons, which is the product of $(1 - w_{L_c}/F) \approx e^{-w_{L_c}/F}$ for each segment. Hence, the probability of exciting a single electron, in a nanotube of length L, with each photon can be estimated by the expression

$$\eta = 1 - \exp\left(\frac{-U(\omega_0)}{F} \int_{-L/2}^{L/2} ds |A_{||}^{+}(s)|^2\right). \quad (43)$$

Note that this expression is actually independent of the coherence length.

Broadening effects can be included in this by substituting the Dirac delta function from Eq. (42) with a Lorentzian function,

$$\delta(E_g - \hbar\omega) \rightarrow \frac{\Gamma}{\pi((E_g - \hbar\omega)^2 + \Gamma^2)}, \quad (44)$$

which has a broadening parameter, Γ. This parameter can include the broadening due to multiple effects, including the electronic state's decay. In carbon nanotubes the state decay occurs on a picosecond time scale.[50] If we take a range of 0.1 ps to 2 ps the required broadening ranges from $\Gamma = 0.01$ eV to $\Gamma = 0.001$ eV. In order to compare our results with previous work[25,51] we will choose in the following to use a parameter of $\Gamma = 0.01$ eV.

So far we have assumed the light to be in a pure state consisting of one specific wavelength. We expect to have a range of wavelengths present and to deal with this we assume the light is in a probabilistic mixture of coherent beams, each with a photon flux F. These are weighted by a line shape $g(\omega)$, satisfying $\int d\omega g(\omega) = 1$. The light's state is then $\int d\omega g(\omega) |\alpha_\omega\rangle\langle\alpha_\omega|$ and the expected absorption probability is

$$\overline{\eta} = \int d\omega g(\omega) \eta. \quad (45)$$

In the following we take g to be a uniform line shape between two energy values. This is equivalent to taking $\overline{\eta}$ to be the average transition probability over a range of energies.

IV. OPTICAL NANOFIBER PHOTON ABSORPTION INTO A CARBON NANOTUBE

We now extend the calculation for the absorption around optical fibers and particularly nanofibers.[52,53] A review of these subwavelength-diameter waveguides can be found in Refs. 54–56. They are made of a silica core and have diameters as small as 50 nm. For fibers of this size a high proportion of the light field exists outside of the fiber's core. This means the field is easily accessible and we consider positioning the carbon nanotube near the nanofiber. The use of fibers allows the interaction to be enhanced due to the transverse confinement of the field. Altering the nanofiber's properties also allows us to tailor the field. Fibers with a smaller diameter have a larger evanescent field but also suffer from higher losses. We will consider a cylindrical nanofiber core with a radius of R and cladding provided by the vacuum, with refractive index $n_2 = 1$. The refractive index of the silica core is $n_1 = 1.45$ and the material absorption of the silica is negligible over the short distances being considered. Silica core fibers with subwavelength diameter are single-mode fibers; i.e., the only mode present is the HE fundamental mode (see Ref. 56 for a general single-mode condition). We make the assumption that the field can be described by the bare fiber mode. In order to validate this assumption we have shown that the nanotube's influence on the field is small. To do this we treated the nanotube as a dielectric cylinder, acting as a separate waveguide, and analyzed the combined mode of the system, using methods based on those found in Ref. 57. In the following we will adopt a scheme used in Refs. 34 and 46 to quantize the field. The field potential operator for the nanofiber's fundamental mode is then

$$\hat{\mathbf{A}}_\omega^+ = \sum_{fp} \sqrt{\frac{\hbar\beta'}{4\pi\omega\epsilon_0 A}} \hat{a}_m \mathbf{e}^m(r,\varphi) e^{i(f\beta z + p\varphi)}. \quad (46)$$

This is given in terms of cylindrical coordinates, with z being the coordinate along the fiber and φ the azimuthal angle. The light's angular frequency is ω. Its propagation direction is labeled with $f = \pm 1$ and β refers to the longitudinal propagation constant. We find the value of β by numerically solving the fiber eigenvalue equation [see Eq. (B1) in Appendix B]. The derivative in Eq. (46), β', is taken with respect to ω, and $\hat{a}_m$ are the photon annihilation operators, with $m = (\omega, f, p)$ characterizing the separate modes. Furthermore, $\mathbf{e}^m$ are the electric field profiles of the guided mode that can be found by solving Maxwell's equations[34,58] and A gives a normalization factor. The expressions for the mode profiles and A are given in Appendix B. The polarization can be right or left circular labeled by $p = \pm 1$. For a single mode of monochromatic coherent light with $m = (\omega_0, f, p)$ we have

$$\mathbf{A}^+ = \sqrt{\frac{F\hbar\beta'}{2\omega_0\epsilon_0 A}} \mathbf{e}^m(r,\varphi) e^{i(f\beta z + p\varphi)}. \quad (47)$$

Figure 6 provides a slice of the classical field at one instant in time. This field can be seen to extend far away from the nanofiber and vary dramatically with position.

This contrasts with the simpler case that has previously been studied of a plane linearly polarized light beam that is given by

$$\hat{\mathbf{A}}_\omega^+ = \sqrt{\frac{\hbar}{4\pi\omega\epsilon_0 c A'}} \hat{a}_\omega \mathbf{e}_z \quad (48)$$
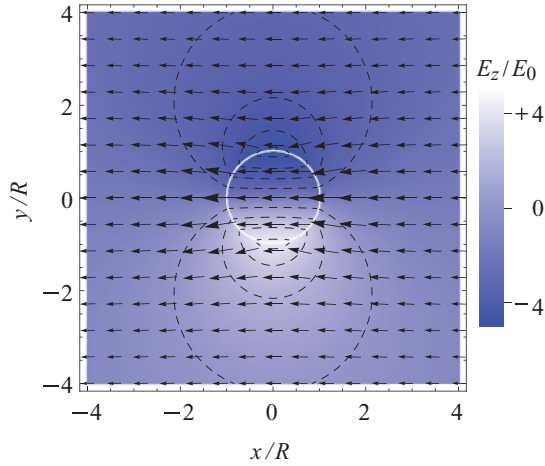
FIG. 6. (Color online) The electric field $\mathbf{E}$ of the circularly polarized HE mode taken for a constant z, to give a cross-section of the fiber. The color gives E_z and the arrows represent the x and y components. The longer the arrow the stronger the field. The field has been divided by the constant $E_0 = \sqrt{F\omega_0\hbar\beta'/(2\epsilon_0 A)}$. Contours (dashed line) for values of E_z/E_0 equal to ± 4, ± 3, ± 2, and ± 1 have been included. In this particular case we took the fiber diameter to be 250 nm and the light's wavelength as 868 nm.

across the whole nanotube, where the beam has a finite cross-sectional area of A'. This gives

$$\mathbf{A}^+ = \sqrt{\frac{F\hbar}{2\omega_0\epsilon_0 c A'}}\mathbf{e}_z. \tag{49}$$

For fibers larger than 100 nm in diameter the photon losses are small and can be ignored over short distances. In our calculations we will use nanofibers of diameter 250 nm. Furthermore, we will focus on the forward propagation and right-polarized guided modes; i.e., $f = p = +1$. All other modes are related to our results by symmetry. The value of G is then highly dependent on the way the nanotube is orientated relative to the nanofiber and can be calculated to be

$$G = \sqrt{\frac{F\hbar\beta'}{2\omega_0\epsilon_0 A}}\langle\Psi^c(\mathbf{k}')|\mathbf{e}^m\exp^{i(f\beta z+p\varphi)}\cdot\nabla|\Psi^v(\mathbf{k})\rangle. \tag{50}$$

Since the field strength drops off exponentially the highest value for the coupling will be achieved by having the nanotube as close as possible to the fiber. In our examples, the distance between the nanotube's center and the surface of the nanofiber is chosen to be 1.25 nm. The nanotubes we consider always have a radius less than 1 nm so this distance avoids any contact. This is so that we do not need to consider surface interactions. These interactions can influence the band structure, particularly by distorting the structure of the nanotube, and may change the nanotube's transport properties. The band structure would still experience a shift due to the van der Waals interactions. However, even in the case of a nanotube placed directly on top of a substrate, with distortion, the bands are shifted by less than 100 meV.[59]

There are two orientations we will consider. The first is that of a straight nanotube, of length L, oriented at an angle ϕ relative to the nanofiber which includes parallel
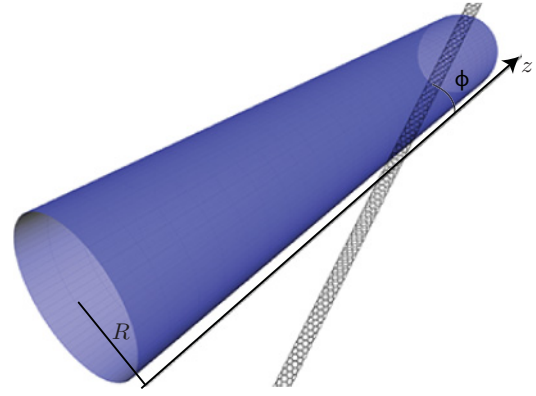

FIG. 7. (Color online) Possible orientations of a straight nanotube relative to a fiber of radius R and positioned parallel to the z axis. ϕ labels the angle between the nanofiber and nanotube.

and perpendicular orientations as illustrated in Fig. 7. For 2 μm nanotubes perpendicular to the fiber, the absorption probabilities as defined by Eq. (43) for different wavelengths of light and different zigzag nanotubes are shown in Fig. 8. We do not consider the absorption of photons with energies greater than 6 eV since these are not visible and require the addition of the higher energy σ orbitals for accurate results. Distinct absorption peaks are clearly visible and the largest absorption occurs for a (11,0) nanotube. The absorption for a nanotube in a linearly polarized coherent plane wave [see Eq. (48)] is also shown in Fig. 8. This beam has a cross-sectional area of 4 μm^2 and exhibits the same absorption peaks as the fiber, but varies less with the light's frequency. It can be seen that the (11,0) nanotube has its smallest energy transition dramatically reduced. This extra effect is caused due to larger evanescent fields, for an increasing wavelength relative to the fiber radius. This reduces the field intensity and absorption. The quantum efficiencies are a similar order of magnitude as those observed experimentally for plane waves.[16,49,60] The different nanotubes show shifted absorption peaks. These can be further adjusted with external fields or choosing other nanotubes.[6–8] The resonant energy values are unchanged with the orientation and this allows us to choose a range to average over as a general measure of absorption. We chose to calculate the mean absorption $\bar{\eta}$ over the (7,0) nanotube's lowest absorption energy; particularly we chose a range of 1 eV from 1.3 eV (953 nm) to 2.3 eV (539 nm). The resulting $\bar{\eta}$ is approximately independent of Γ in a range of $\Gamma = 0.01$ eV to $\Gamma = 0.001$ eV deviating only by a few percent.

The corresponding mean absorption against nanotube length, for the lowest energy transition, is shown in Fig. 9 for various angles between the straight nanotube and nanofiber. The results show that the absorption converges to a maximum value as the length is increased, unless the nanotube is parallel to the fiber. The nanotube perpendicular to the fiber has a very strong absorption for short lengths. In this situation we see the absorption increasing strongly with nanotube length which is due to the linear increase in electron number. As the length increases further this effect is counterbalanced by the fact that the field strength decreases exponentially away from the nanofiber. The absorption hardly increases at all
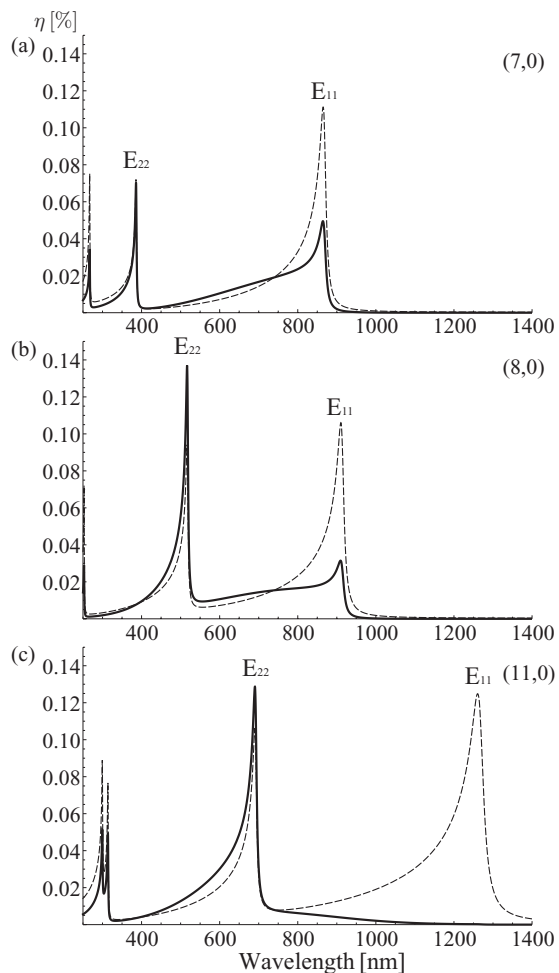
FIG. 8. Photon absorption probabilities η for a 2 μm long nanotube, perpendicular to the fiber, at different photon energies. The nanotubes considered are (a) (7,0), (b) (8,0), and (c) (11,0). In each case the solid lines refer to the absorption of circularly polarized light guided by the nanofiber and the dashed lines represent the absorption for a plane coherent light beam (without a fiber) that is linearly polarized along the nanotube. The two lowest energy transitions, E_{11} and E_{22}, are indicated. We have used a broadening parameter of $\Gamma = 0.01$ eV.

after the nanotube exceeds approximately 2 μm. However, over these short distances the absorption of the perpendicular nanotube can be improved upon by shifting the nanotube slightly away from a perfectly perpendicular arrangement. The parallel orientation increases slowly but does not peak. This effect will be discussed later in this section and we will find that the probability can be enhanced by spiraling the nanotube to combine both effects. This can be qualitatively understood by noting that the evanescent field is elliptically polarized; however the plane containing the ellipse is not perpendicular to the fiber. Instead, it is inclined so the absorption is enhanced by aligning the nanotube such that it lies within the plane. If linear-polarized light was used instead of circular-polarized light the absorption could be twice as high depending on the nanotube's position in the nanofiber plane. We also see a difference between angles of $\pm\pi/32$, with the higher
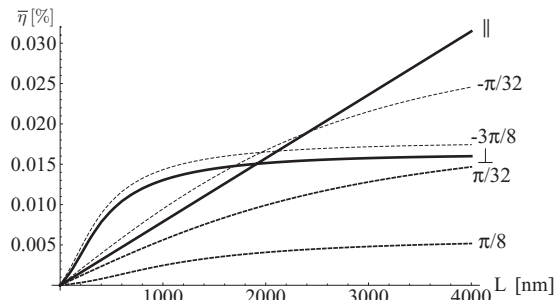

FIG. 9. Average photon absorption probability $\overline{\eta}$ for a straight (7,0) nanotube of length L. At $L = 4\,\mu$m the angles between nanotube and fiber are $\phi = 0$ (parallel), $-\pi/32$, $-3\pi/8$, $\pi/2$ (perpendicular), $\pi/32$, $\pi/8$. The mean absorption has been taken over a 1 eV region, from 1.3 eV to 2.3 eV.

absorption being dependent on the light's polarization and propagation.

The strong absorption for a perpendicular nanotube is limited by the drop-off in field strength. However, this can be prevented by maintaining a constant distance between the nanotube and nanofiber center, R_n. The nanotube can locally approximate a perpendicular nanotube by spiraling around the nanofiber, as illustrated in Fig. 10. Although this bending does alter the electronic and optical properties these effects are small and can be safely ignored here.[61] We define a "winding number," W, for the spiral as the number of loops per unit length along the z axis. This winding number is equal to $W = 1/d_l$ where d_l is the z distance for one loop. An angle is also formed between the spiralling nanotube and the nanofiber's direction, which is given by $\Phi_s = \arctan(2\pi W R_n)$. Since these spiralling nanotubes can interact with the field over an arbitrary length their absorptions approach 100% given sufficient length and an allowed transition.

The average absorption probabilities in this case are plotted in Fig. 11 and show a steady increase in the absorption probability with nanotube length. The parallel nanotube is also shown. This demonstrates that the spiralling nanotubes can have higher absorption probabilities than the parallel configuration. In Fig. 12 we have plotted the average absorption probability against Φ_s for nanotubes of different lengths.
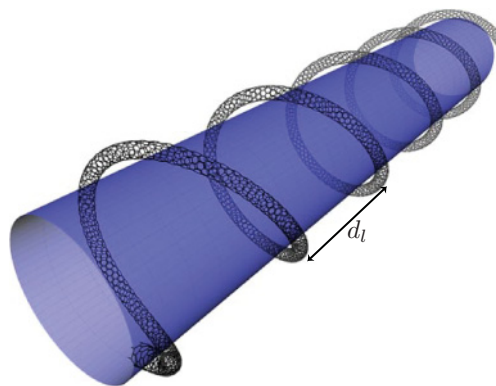

FIG. 10. (Color online) Nanotube spiraling around a nanofiber. The length of one loop, along the z axis, is labeled as d_l.
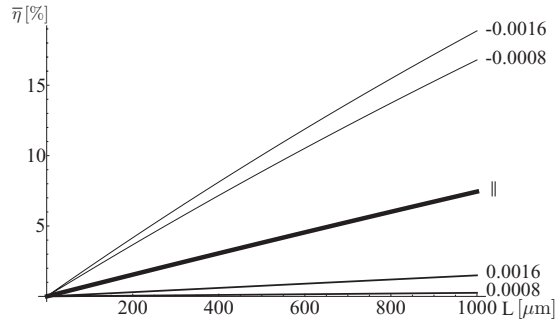
FIG. 11. Average photon absorption probability $\overline{\eta}$ for a (7,0) nanotube of length L coiled around the fiber. The average is taken from 1.3 eV to 2.3 eV. The winding numbers are -0.0016 nm^{-1}, -0.0008 nm^{-1}, 0 nm^{-1} (parallel), 0.0016 nm^{-1}, and 0.0008 nm^{-1}.

An optimal spiraling rate to enhance the absorption can be seen. We found that the optimal value of this winding rate is $W_{\mathrm{opt}} = e_\varphi^m / (2\pi R_n e_z^m)$. This was obtained by maximizing the alignment between the nanotube and $\mathbf{e}^m$. Note that W_{opt}, and hence the optimal Φ_s, is independent of the nanotube used. There is also another coil that lies perpendicular to the optimal one and has near zero absorption. Such nanotubes could have a variety of applications. For example, two semiconducting nanotubes could be prepared to give near-zero absorption for different polarizations of light and then used to distinguish between these polarizations. They would also enable systems of nanotubes to be used as electrical conductors, around the nanofiber, without absorbing photons from the fiber and these could be used as contacts.

V. APPLICATIONS

The nanotube-nanofiber setups discussed in the previous sections open up possibilities for a range of applications, particularly highly sensitive photodetectors. These systems would detect light guided within a fiber. In this section we discuss the possibilities. Note that we have only considered the quantum efficiency of the absorption and that detection
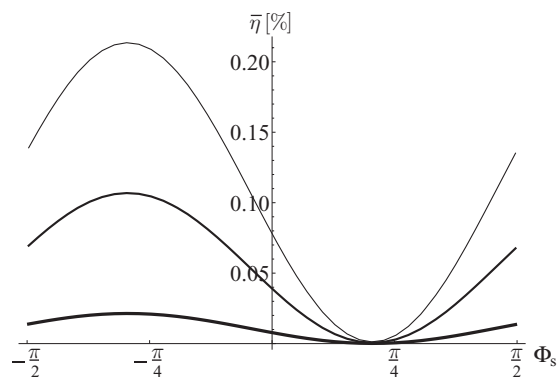

FIG. 12. Average photon absorption probability $\overline{\eta}$ for (7,0) nanotubes coiled around the fiber for different winding parameters. From top to bottom the nanotubes have lengths 10 000 nm, 5000 nm, and 1000 nm. The average is taken from 1.3 eV to 2.3 eV.
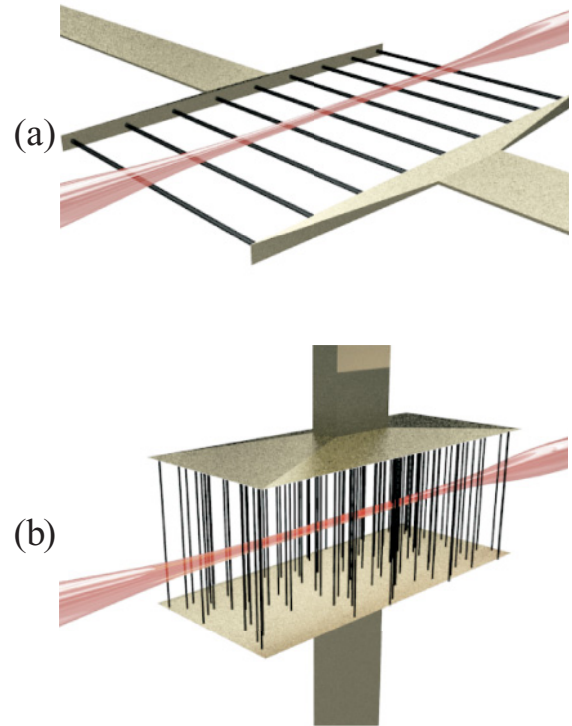

FIG. 13. (Color online) Illustrations of possible photodetectors. Once the light field excites an electron the resistance between the electrodes drops dramatically, which allows the photon to be recorded. (a) A horizontal array of aligned nanotubes (thick dark lines) are formed between two electrodes and the nanofiber is then laid perpendicular to these nanotubes. (b) Here a "forest" of aligned semiconducting nanotubes are grown between two electrodes. The nanofiber is positioned between these electrodes.

of the charge excitations is beyond the scope of this paper. However, certain nanotube properties such as ballistic electron transport and low capacitance should be a great advantage for this detection. The band gap of carbon nanotubes decreases with the nanotube size, so for optical and near-infrared wavelengths small-diameter nanotubes are required. This rules out the possibility of encasing a nanofiber within a nanotube. Instead, a practical setup is given by arranging N horizontal nanotubes in a parallel array and placing the nanofiber orthogonally on top of the array [see Fig. 13(a)]. Based on current nanotube arrays, the density of nanotubes would be 1–100 nanotubes per μm.[62–66] We will use $\overline{\eta}$ as a measure of the absorption probability for one nanotube. The photon absorption probability of each nanotube is then, in the case of a (7,0) nanotube, given in Fig. 9 and the overall absorption probability is

$$\eta_{\mathrm{tot}} = 1 - (1 - \overline{\eta})^N. \qquad (51)$$

Taking $\overline{\eta} = 0.000\,15$ (see Fig. 9) this leads to $\eta_{\mathrm{tot}} > 95\%$ for $N > 20\,000$, a value greatly exceeding those of currently available avalanche photodiodes (APDs).[67] For $N > 40\,000$ the efficiency exceeds 99% which can currently only be achieved by highly complex superconducting detectors.[67] The
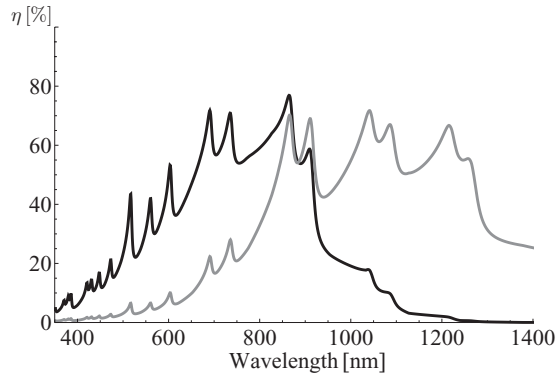
FIG. 14. Absorption probability for a circularly polarized photon in a nanofiber laid inside a "forest" of nanotubes (see Fig. 13). This is given for 2 μm long vertically aligned nanotubes. The nanotubes are in a region that extends 500 nm away from the fiber and 15 μm along its length. The density of the array is taken as 900 nanotubes per μm^2. The fiber's diameter is taken to be either 250 nm (black line) or 400 nm (gray line). A broadening parameter of $\Gamma = 0.01$ eV was used.

advantage of our setup is that it can be operated at room temperature. Each nanotube would require a length of 2 μm and has to be connected at the ends by electrodes[68] which collect the excited electrons via an applied voltage. Although this should be possible in the near future, current technology cannot generate an array of unique nanotubes.

Aligned vertical nanotubes can also be grown on a conducting substrate, which can then serve as one electrode. The nanofiber can then be placed orthogonally to the nanotubes and the remaining ends of the nanotubes connected to an additional electrode [see Fig. 13(b)]. The diameter of the nanotubes in this case can be in the range of 1 ± 0.5 nm.[69,70] Recently, progress has been made in the generation of such semiconducting nanotube "forests," although a semiconducting nanotube purity of 100% has yet to be achieved reliably.[71–73] These nanotube systems typically have a density of 10–10 000 nanotubes per μm^2.[74–77] The nanotubes are distributed uniformly over a selected region and we assume that they are a uniform mix of semiconducting zigzag nanotubes with a diameter in the range 1 ± 0.5 nm. We calculated the overall absorption probability when we have a forest that extends a distance of 500 nm from the nanofiber and 15 μm along its length, with a density of 900 nanotubes per μm^2. The results with nanofibers that have diameters of 250 nm and 400 nm are shown in Fig. 14. These absorb light of a wide range of wavelengths, which can be selected by the nanotubes present and choice of nanofiber diameter. A typical absorption probability of $\eta_{tot} > 50\%$ can be seen, for 250 nm diameter fibers, and by extending the system's length from 15 μm to 50 μm this is increased to $\eta_{tot} > 95\%$. Nanotubes around a 400 nm fiber are also seen to absorb light at wavelengths that are typically used for optical communication. Due to the nanotube's band gap dependence on external fields there is also the possibility of adjusting the absorption frequencies by using an external field.

An additional possible setup is given by arranging the nanofiber and the nanotube parallel to each other. Taking 100 nanotubes of length $L = 1$ mm parallel to the fiber and

using $\overline{\eta} = 0.07$ (see Fig. 11) we obtain an overall absorption probability of $\eta_{tot} > 99\%$ which again greatly exceeds that of standard APDs.

As a final setup we consider the coil geometry shown in Fig. 10 which has a high absorption probability of up to 100% for long nanotubes. However, producing such a setup in a laboratory is rather challenging with current technology. This setup also allows for further specification of the absorbed light's polarization or propagation direction with the choice of winding number. The winding also dramatically reduces the length of the system. For a nanotube with a winding number of $W = -0.1$ nm^{-1}, the average absorption between 1.5 eV and 2.5 eV exceeds 50% when the nanotube's length is 5 mm. For the 250 nm diameter fiber this only extends 64 μm along the fiber.

VI. SUMMARY

In this paper we have calculated the probability of absorbing a photon with zigzag carbon nanotubes. The light field is allowed to vary along the nanotube; i.e., no dipole approximation is made, which has enabled us to treat the absorption of light from optical nanofibers. We found that there is a strong dependence on the system's geometry and have devised setups for high absorption. With a sufficiently long nanotube parallel to the nanofiber, we find that an absorption of circularly polarized light arbitrarily close to 100% can be achieved. This can be further improved on if we spiral the nanotube around the fiber so that the required nanotube length is dramatically reduced. A coiled nanotube can also be engineered so that it does not absorb any light from the nanofiber. For straight nanotubes that are not parallel to the fiber, we find that the absorption probability converges as the nanotube's length increases. However, if multiple perpendicular nanotubes are arranged parallel to the fiber arbitrary absorption can still be achieved. We have found a simple expression for the absorption probability, which is independent of the coherence length. Currently, the coherence lengths of carbon nanotubes is an area of extensive research with results ranging from 10 nm, at room temperature, to a few microns.[28–32] They seem to be highly dependent on the temperature, impurities, defects and surrounding fields. Once excited, the radiative lifetimes of the excitations have been observed to range from 3 to 100 ns.[28,78] The nonradiative decay seems to be much faster, of the order of a few picoseconds.[50] Introducing excitons into the model and analyzing the dynamics of quantized single-photon states within a carbon nanotube is an interesting area of further research. Yet, the results here are an important step towards calculating the absorptions within nanostructures and are of importance to future nanotube optoelectonics.

APPENDIX A: CALCULATING THE OPTICAL MATRIX ELEMENT

The matrix element for the interaction between can be found by substituting in the wave functions to give

$$
\begin{aligned}
G &= \langle \Psi^c(\mathbf{k}') | \mathbf{A}^+ \cdot \nabla | \Psi^v(\mathbf{k}) \rangle \\
&= \sum_{s,t=A,B} c_s^{c*}(\mathbf{k}') c_t^v(\mathbf{k}) \langle \tilde{p}_z^s(\mathbf{k}') | \mathbf{A}^+ \cdot \nabla | \tilde{p}_z^t(\mathbf{k}) \rangle \\
&= \frac{1}{N_{\text{cells}}} \sum_{s,t=A,B} c_s^{c*}(\mathbf{k}') c_t^v(\mathbf{k}) \sum_{\mathbf{r}_1 \in \mathbf{R}_s, \mathbf{r}_2 \in \mathbf{R}_t} e^{i\mathbf{k}\cdot\mathbf{r}_2 - i\mathbf{k}'\cdot\mathbf{r}_1} \langle p_z(\mathbf{r}-\mathbf{r}_1) | \mathbf{A}^+ \cdot \nabla | p_z(\mathbf{r}-\mathbf{r}_2) \rangle \\
&= \frac{1}{N_G N_L} \sum_{\mathbf{r}_1 \in \mathbf{R}_A, \mathbf{r}_2 \in \mathbf{R}_B} c_A^{c*}(\mathbf{k}') c_B^v(\mathbf{k}) e^{i\mathbf{k}\cdot\mathbf{r}_2 - i\mathbf{k}'\cdot\mathbf{r}_1} \langle p_z(\mathbf{r}-\mathbf{r}_1) | \mathbf{A}^+ \cdot \nabla | p_z(\mathbf{r}-\mathbf{r}_2) \rangle \\
&\quad + c_B^{c*}(\mathbf{k}') c_A^v(\mathbf{k}) e^{i\mathbf{k}\cdot\mathbf{r}_1 - i\mathbf{k}'\cdot\mathbf{r}_2} \langle p_z(\mathbf{r}-\mathbf{r}_2) | \mathbf{A}^+ \cdot \nabla | p_z(\mathbf{r}-\mathbf{r}_1) \rangle \\
&= \frac{M\sqrt{3}}{aN_G N_L} \left[c_A^{c*}(\mathbf{k}') c_B^v(\mathbf{k}) \sum_{\mathbf{r}_1 \in \mathbf{R}_A} e^{-i(\mathbf{k}'-\mathbf{k})\cdot\mathbf{r}_1} \mathbf{A}^+(\mathbf{r}_1) \cdot \mathbf{v}^A(\mathbf{k}) + c_B^{c*}(\mathbf{k}') c_A^v(\mathbf{k}) \sum_{\mathbf{r}_2 \in R_B} e^{-i(\mathbf{k}'-\mathbf{k})\cdot\mathbf{r}_2} \mathbf{A}^+(\mathbf{r}_2) \cdot \mathbf{v}^B(\mathbf{k}) \right]. \quad (A1)
\end{aligned}
$$

Here we have assumed that the orbitals are symmetric and that $\mathbf{A}^+$ is constant across each of the nanotube's unit cells. The expression for G can then be split into separate unit cells and directions:

$$
G = G_x + G_y + G_z, \quad (A2)
$$

$$
\begin{aligned}
G_z &= \frac{M\sqrt{3}}{2anN_L} \left[\sum_{l=1}^{N_L} e^{i[al\sqrt{3}-(L/2)](k_\| - k_\|')} A_z^+(la\sqrt{3}-(L/2)) \right] \\
&\quad \times \sum_{j=1}^{n} \left[c_A^{c*}(\mathbf{k}') c_B^v(\mathbf{k}) e^{-ija(k_\perp' - k_\perp)}(1 + e^{-ia(\mathbf{k}'-\mathbf{k})\cdot(\sqrt{3}/2,1/2)}) v_z^A(\mathbf{k}) \right. \\
&\quad \left. - c_B^{c*}(\mathbf{k}') c_A^v(\mathbf{k}) e^{-ija(k_\perp' - k_\perp)} e^{ia(k_\| - k_\|')/\sqrt{3}}(1 + e^{-ia(\mathbf{k}'-\mathbf{k})\cdot(\sqrt{3}/2,1/2)}) v_z^A(\mathbf{k})^* \right] \\
&= \frac{1}{N_L} D_z \left[\sum_{l=1}^{N_L} e^{i(k_\| - k_\|')[la\sqrt{3}-(L/2)]} A_z^+(la\sqrt{3}-(L/2)) \right]. \quad (A3)
\end{aligned}
$$

In order to calculate G_x and G_y we must take the curvature of the nanotube into consideration. To do this we use the method from Ref. 18 and introduce the parameters

$$
v_\pm^{A_0} = e^{ia\mathbf{k}\cdot(-1/(2\sqrt{3}),-1/2)}(e^{\mp 2\pi i/2n} - 1) + e^{ia\mathbf{k}\cdot(-1/(2\sqrt{3}),1/2)}(e^{\pm 2\pi i/2n} - 1), \quad (A4)
$$

$$
v_\pm^{B_0} = e^{ia\mathbf{k}\cdot(1/(2\sqrt{3}),-1/2)}(e^{\mp 2\pi i/2n} - 1) + e^{ia\mathbf{k}\cdot(1/(2\sqrt{3}),1/2)}(e^{\pm 2\pi i/2n} - 1), \quad (A5)
$$

$$
v_{x(\theta)}^A(\mathbf{k}) = R_t \frac{e^{i\theta} v_+^{A_0} + e^{-i\theta} v_-^{A_0}}{2}, \quad (A6)
$$

$$
v_{x(\theta)}^B(\mathbf{k}) = R_t \frac{e^{i\theta} v_+^{B_0} + e^{-i\theta} v_-^{B_0}}{2}, \quad (A7)
$$

$$
v_{y(\theta)}^A(\mathbf{k}) = R_t \frac{e^{i\theta} v_+^{A_0} + e^{-i\theta} v_-^{A_0}}{2i}, \quad (A8)
$$

$$
v_{y(\theta)}^B(\mathbf{k}) = R_t \frac{e^{i\theta} v_+^{B_0} + e^{-i\theta} v_-^{B_0}}{2i}. \quad (A9)
$$

From these we calculate $G_{d=x,y}$ to be

$$
\begin{aligned}
G_d &= \frac{M\sqrt{3}}{2anN_L} \left[\sum_{l=1}^{N_L} e^{i(k_\| - k_\|')[la\sqrt{3}-(L/2)]} A_d^+(la\sqrt{3}-(L/2)) \right] \sum_{j=1}^{n} c_A^{c*}(\mathbf{k}') c_B^v(\mathbf{k}) \big(v_{d(2\pi j/n)}^A(\mathbf{k}) e^{-ija(k_\perp' - k_\perp)} \\
&\quad + v_{d[2\pi(j+1/2)/n]}^A(\mathbf{k}) e^{-ija(k_\perp' - k_\perp)} e^{-ia\mathbf{k}'\cdot(1/(2\sqrt{3}),1/2)} \big) - c_B^{c*}(\mathbf{k}') c_A^v(\mathbf{k}) \big(v_{d(2\pi j/n)}^B(\mathbf{k}) e^{-ija(k_\perp' - k_\perp)} e^{-iak_\|'/\sqrt{3}} \\
&\quad + v_{d[2\pi(j+1/2)/n]}^B(\mathbf{k}) e^{-ija(k_\perp' - k_\perp)} e^{-ia\mathbf{k}'\cdot(5/(2\sqrt{3}),1/2)} \big) \\
&= \frac{1}{N_L} \mathbf{D}_d \left[\sum_{l=1}^{N_L} e^{i(k_\| - k_\|')[la\sqrt{3}-(L/2)]} A_d^+(la\sqrt{3}-(L/2)) \right]. \quad (A10)
\end{aligned}
$$

Hence, we obtain

$$G = \frac{1}{N_L} \mathbf{D} \sum_{l=1}^{N_L} e^{i(k_{\parallel} - k_{\parallel}')[la\sqrt{3} - (L/2)]} \mathbf{A}^{+}(la\sqrt{3} - (L/2)). \tag{A11}$$

"

APPENDIX B: CLASSICAL NANOFIBER FIELD MODES

For light of wavelength λ and $k = 2\pi/\lambda$, the field parameters must satisfy the fiber eigenvalue equation[58]

$$\frac{J_0(hR)}{hRJ_1(hR)} = -\frac{n_1^2 + n_2^2}{2n_1^2} \frac{K_1'(qR)}{qRK_1(qR)} + \frac{1}{h^2R^2} - \left[\left(\frac{n_1^2 - n_2^2}{2n_1^2} \frac{K_1'(qR)}{qRK_1(qR)} \right)^2 + \frac{\beta^2}{n_1^2k^2} \left(\frac{1}{q^2R^2} + \frac{1}{h^2R^2} \right)^2 \right]^{1/2}, \tag{B1}$$

with J_ν referring to the Bessel function of the first kind and K_ν being the modified Bessel function of the second kind. By numerically solving Eq. (B1) the value of the propagation constant β is determined. We also define the parameters $h = (n_1^2k^2 - \beta^2)^{1/2}$, $q = (\beta^2 - n_2^2k^2)^{1/2}$, and

$$g = \left(\frac{1}{q^2R^2} + \frac{1}{h^2R^2} \right) \Bigg/ \left(\frac{J_1'(hR)}{hRJ_1(hR)} + \frac{K_1'(qR)}{qRK_1(qR)} \right). \tag{B2}$$

Inside the fiber $(0 < r < R)$ the guided mode, $m = (f, p)$, has the form

$$e_r^m = i\frac{qK_1(R)}{hJ_1(hR)}[(1-g)J_0(hr) - (1+g)J_2(hr)], \tag{B3}$$

$$e_\varphi^m = -p\frac{qK_1(qR)}{hJ_1(hR)}[(1-g)J_0(hr) + (1+g)J_2(hr)], \tag{B4}$$

$$e_z^m = f\frac{2qK_1(qR)}{\beta J_1(hR)}J_1(hr), \tag{B5}$$

and outside $r > R$

$$e_r^m = i[(1-g)K_0(qr) + (1+g)K_2(qr)], \tag{B6}$$

$$e_\varphi^m = -p[(1-g)K_0(qr) - (1+g)K_2(qr)], \tag{B7}$$

$$e_z^m = f\frac{2q}{\beta}K_1(qr). \tag{B8}$$

These are normalized with a factor given by

$$\int_0^{2\pi} \int_0^R n_1^2 |\mathbf{e}|^2 r\,dr\,d\varphi + \int_0^{2\pi} \int_R^\infty n_2^2 |\mathbf{e}|^2 r\,dr\,d\varphi = A. \tag{B9}$$

[1] J.-C. Charlier, X. Blase, and S. Roche, Rev. Mod. Phys. **79**, 677 (2007).

[2] T. Ando, J. Phys. Soc. Jpn. **74**, 777 (2005).

[3] R. Saito, G. Dresselhaus, and M. Dresselhaus, *Physical Properties of Carbon Nanotubes* (Imperial College Press, London, 1998).

[4] X. Wang, Q. Li, J. Xie, Z. Jin, J. Wang, Y. Li, K. Jiang, and S. Fan, Nano Lett. **9**, 3137 (2009).

[5] C. White and T. Todorov, Nature (London) **393**, 240 (1998).

[6] J. Klinovaja, M. J. Schmidt, B. Braunecker, and D. Loss, Phys. Rev. Lett. **106**, 156809 (2011).

[7] Y.-H. Kim and K. J. Chang, Phys. Rev. B **64**, 153404 (2001).

[8] M. Pacheco, Z. Barticevic, C. G. Rocha, and A. Latgé, J. Phys.: Condens. Matter **17**, 5839 (2005).

[9] I. Takesue, J. Haruyama, N. Kobayashi, S. Chiashi, S. Maruyama, T. Sugai, and H. Shinohara, Phys. Rev. Lett. **96**, 057001 (2006).

[10] J. Noffsinger and M. L. Cohen, Phys. Rev. B **83**, 165420 (2011).

[11] A. Y. Kasumov, R. Deblock, M. Kociak, B. Reulet, H. Bouchiat, I. I. Khodos, Y. B. Gorbatov, V. T. Volkov, C. Journet, and M. Burghard, Science **284**, 1508 (1999).

[12] A. F. Morpurgo, J. Kong, C. M. Marcus, and H. Dai, Science **286**, 263 (1999).

[13] K. Uchida and S. Okada, Phys. Rev. B **79**, 085402 (2009).

[14] E. S. Snow, F. K. Perkins, E. J. Houser, S. C. Badescu, and T. L. Reinecke, Science **307**, 1942 (2005).

[15] X. Tang, S. Bansaruntip, N. Nakayama, E. Yenilmez, Y.-l. Chang, and Q. Wang, Nano Lett. **6**, 1632 (2006).

[16] M. Freitag, Y. Martin, J. A. Misewich, R. Martel, and P. Avouris, Nano Lett. **3**, 1067 (2003).

[17] C. D. Spataru, S. Ismail-Beigi, L. X. Benedict, and S. G. Louie, Phys. Rev. Lett. **92**, 077402 (2004).

[18] J. Jiang, R. Saito, A. Grüneis, G. Dresselhaus, and M. Dresselhaus, Carbon **42**, 3169 (2004).

[19]S. Motavas, A. Ivanov, and A. Nojeh, Phys. Rev. B **82**, 085442 (2010).

[20]A. Zarifi and T. G. Pedersen, Phys. Rev. B **80**, 195422 (2009).

[21]S. V. Goupalov, A. Zarifi, and T. G. Pedersen, Phys. Rev. B **81**, 153402 (2010).

[22]S. V. Goupalov, Phys. Rev. B **72**, 195403 (2005).

[23]S. Berciaud, C. Voisin, H. Yan, B. Chandra, R. Caldwell, Y. Shan, L. E. Brus, J. Hone, and T. F. Heinz, Phys. Rev. B **81**, 041414 (2010).

[24]Y. Takagi and S. Okada, Phys. Rev. B **79**, 233406 (2009).

[25]A. Zarifi and T. G. Pedersen, Phys. Rev. B **74**, 155434 (2006).

[26]E. Malić, M. Hirtschulz, F. Milde, A. Knorr, and S. Reich, Phys. Rev. B **74**, 195431 (2006).

[27]R. Saito, A. Gruneis, G. Samsonidze, G. Dresselhaus, M. Dresselhaus, A. Jorio, L. Cancado, M. Pimenta, and A. Souza, Appl. Phys. A **78**, 1099 (2004).

[28]Y. Miyauchi, H. Hirori, K. Matsuda, and Y. Kanemitsu, Phys. Rev. B **80**, 081410 (2009).

[29]S. Roche, J. Jiang, F. Triozon, and R. Saito, Phys. Rev. Lett. **95**, 076803 (2005).

[30]S. Tans, M. Devoret, H. Dai, A. Thess, R. Smalley, L. Geerligs, and C. Dekker, Nature (London) **386**, 474 (1997).

[31]S. Roche, J. Jiang, F. Troizon, and R. Saito, Phys. Rev. B **72**, 113410 (2005).

[32]V. Perebeinos, J. Tersoff, and P. Avouris, Phys. Rev. Lett. **94**, 086802 (2005).

[33]J. Bures and R. Ghosh, J. Opt. Soc. Am. A **16**, 1992 (1999).

[34]F. Le Kien, S. Dutta Gupta, K. P. Nayak, and K. Hakuta, Phys. Rev. A **72**, 063815 (2005).

[35]G. Sagué, E. Vetsch, W. Alt, D. Meschede, and A. Rauschenbeutel, Phys. Rev. Lett. **99**, 163602 (2007).

[36]E. Vetsch, D. Reitz, G. Sagué, R. Schmidt, S. T. Dawkins, and A. Rauschenbeutel, Phys. Rev. Lett. **104**, 203603 (2010).

[37]A. Liao, Y. Zhao, and E. Pop, Phys. Rev. Lett. **101**, 256804 (2008).

[38]M. S. Dresselhaus, G. Dresselhaus, R. Saito, and A. Jorio, Annu. Rev. Phys. Chem. **58**, 719 (2007).

[39]J. E. Bunder and J. M. Hill, Phys. Rev. B **80**, 153406 (2009).

[40]A. D. Mohite, P. Gopinath, H. M. Shah, and B. W. Alphenaar, Nano Lett. **8**, 142 (2008).

[41]M. Ichida, S. Mizuno, Y. Tani, Y. Saito, and A. Nakamura, J. Phys. Soc. Jpn. **68**, 3131 (1999).

[42]D. Abergel, V. Apalkov, J. Berashevich, K. Ziegler, and T. Chakraborty, Adv. Phys. **59**, 261 (2010).

[43]A. Grüneis, R. Saito, G. G. Samsonidze, T. Kimura, M. A. Pimenta, A. Jorio, A. G. Souza Filho, G. Dresselhaus, and M. S. Dresselhaus, Phys. Rev. B **67**, 165402 (2003).

[44]R. Saito, G. Dresselhaus, and M. S. Dresselhaus, Phys. Rev. B **61**, 2981 (2000).

[45]A. V. Nikolaev, A. V. Bibikov, A. V. Avdeenkov, I. V. Bodrenko, and E. V. Tkalya, Phys. Rev. B **79**, 045418 (2009).

[46]K. J. Blow, R. Loudon, S. J. D. Phoenix, and T. J. Shepherd, Phys. Rev. A **42**, 4102 (1990).

[47]S. Tasaki, K. Maekawa, and T. Yamabe, Phys. Rev. B **57**, 9301 (1998).

[48]H. Ajiki and T. Ando, Physica B (Amsterdam) **201**, 349 (1994).

[49]M. F. Islam, D. E. Milkie, C. L. Kane, A. G. Yodh, and J. M. Kikkawa, Phys. Rev. Lett. **93**, 037404 (2004).

[50]J.-S. Lauret, C. Voisin, G. Cassabois, C. Delalande, P. Roussignol, O. Jost, and L. Capes, Phys. Rev. Lett. **90**, 057404 (2003).

[51]M. F. Lin, Phys. Rev. B **62**, 13153 (2000).

[52]L. Tong, R. Gattass, J. Ashcom, S. He, J. Lou, M. Shen, I. Maxwell, and E. Mazur, Nature (London) **426**, 816 (2003).

[53]L. Tong and E. Mazur, J. Non-Cryst. Solids **354**, 1240 (2008).

[54]G. Brambilla, V. Finazzi, and D. Richardson, Opt. Express **12**, 2258 (2004).

[55]L. Tong, Front. Optoelectron. China **3**, 54 (2010).

[56]L. Tong, J. Lou, and E. Mazur, Opt. Express **12**, 1025 (2004).

[57]A. W. Snyder and W. R. Young, J. Opt. Soc. Am. **68**, 297 (1978).

[58]A. Snyder and J. Love, *Optical Waveguide Theory*, Science Paperbacks (Chapman and Hall, London, 1983).

[59]J. S. Soares and A. Jorio, J. Nanotechnol. **2012**, 512738 (2012).

[60]S. Berciaud, L. Cognet, and B. Lounis, Phys. Rev. Lett. **101**, 077402 (2008).

[61]P. Koskinen, Phys. Rev. B **82**, 193409 (2010).

[62]L. Ding, A. Tselev, J. Wang, D. Yuan, H. Chu, T. P. McNicholas, Y. Li, and J. Liu, Nano Lett. **9**, 800 (2009).

[63]C. Wang, K. Ryu, L. De Arco, A. Badmaev, J. Zhang, X. Lin, Y. Che, and C. Zhou, Nano Res. **3**, 831 (2010).

[64]B. K. Sarker, S. Shekhar, and S. I. Khondaker, ACS Nano **5**, 6297 (2011).

[65]S. W. Hong, T. Banks, and J. A. Rogers, Adv. Mater. **22**, 1826 (2010).

[66]S. Shekhar, P. Stokes, and S. I. Khondaker, ACS Nano **5**, 1739 (2011).

[67]R. H. Hadfield, Nat. Photonics **3**, 696 (2009).

[68]H. Wang, J. Luo, F. Schäffel, M. H. Rümmeli, G. A. D. Briggs, and J. H. Warner, Nanotechnology **22**, 245305 (2011).

[69]Y.-Q. Xu, E. Flor, M. J. Kim, B. Hamadani, H. Schmidt, R. E. Smalley, and R. H. Hauge, J. Am. Chem. Soc. **128**, 6560 (2006).

[70]M. G. Hahm, Y.-K. Kwon, E. Lee, C. W. Ahn, and Y. J. Jung, J. Phys. Chem. C **112**, 17143 (2008).

[71]P. Li and J. Zhang, J. Mater. Chem. **21**, 11815 (2011).

[72]L. Qu, F. Du, and L. Dai, Nano Lett. **8**, 2682 (2008).

[73]P. G. Collins, M. S. Arnold, and P. Avouris, Science **292**, 706 (2001).

[74]G. F. Zhong, T. Iwasaki, and H. Kawarada, Carbon **44**, 2009 (2006).

[75]Y. Murakami, S. Chiashi, Y. Miyauchi, M. Hu, M. Ogura, T. Okubo, and S. Maruyama, Chem. Phys. Lett. **385**, 298 (2004).

[76]S. Esconjauregui, M. Fouquet, B. C. Bayer, C. Ducati, R. Smajda, S. Hofmann, and J. Robertson, ACS Nano **4**, 7431 (2010).

[77]I. Ibrahim, A. Bachmatiuk, F. Börrnert, J. Blüher, U. Wolff, J. H. Warner, B. Büchner, G. Cuniberti, and M. H. Rümmeli, Carbon **49**, 5029 (2011).

[78]F. Wang, G. Dukovic, L. E. Brus, and T. F. Heinz, Phys. Rev. Lett. **92**, 177401 (2004).